ChemPhysChem

Research Article
doi.org/10.1002/cphc.202300379

Chemistry Europe
European Chemical Societies Publishing

www.chemphyschem.org

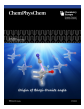

Origin of the Bürgi-Dunitz Angle

Humberto A. Rodríguez,[a, b] F. Matthias Bickelhaupt,[c] and Israel Fernández*[a]

The Bürgi-Dunitz (BD) angle plays a pivotal role in organic chemistry to rationalize the nucleophilic addition to carbonyl groups. Yet, the origin of the obtuse trajectory of the nucleophile remains incompletely understood. Herein, we quantify the importance of the underlying physical factors quantum chemically. The obtuse BD angle appears to originate from the concerted action of a reduced Pauli repulsion between the nucleophile HOMO and carbonyl π bond, a more stabilizing HOMO-π*-LUMO(C=O) interaction, as well as a more favorable electrostatic attraction.

Introduction

In the 1970s, Bürgi and Dunitz deduced, from the analysis of a number of crystal structures containing an amine and a proximal carbonyl, that the angle θ of approach of a nucleophile to a carbonyl group in the corresponding transition structure was obtuse (105 ± 5°) and not perpendicular (90°).[1–3] This was confirmed at that time by SCF-LCAO calculations on the approach of a hydride anion (H^-) to formaldehyde, which provided an angle of attack of 107°.[1] Since then, the so-called Bürgi-Dunitz (BD) angle has played a crucial role in organic chemistry[4] and was used, for instance, to rationalize the stereoselectivity in nucleophilic additions to carbonyl groups,[5] the structural stability of proteins,[6] and related systems featuring intra- or intermolecular n→π*(C=O)[7] or π-hole interactions,[8] which are reminiscent of the BD trajectory.

Despite its relevance, the origin of the BD angle is still incompletely understood. Based on Frontier Molecular Orbital (FMO) theory[9] and the asymmetry of the π*-LUMO (in terms of MO-coefficients) of the carbonyl group,[4,5,10] the angle of attack is typically explained in textbooks as *"the result of a compromise between maximum orbital overlap for the stabilizing HOMO(nucleophile)-π*-LUMO(C=O)* [i.e., for θ = 90°] *and minimum repulsion with the electron density in the carbonyl π-bond* [i.e., for θ > 90°]".[11] In this sense, the earlier work by Stone and Erskine using an implementation of Basilevsky and Berenfeld's intermolecular SCF perturbation theory with the minimal STO-3G basis-set should be highlighted[12] as they found that a frontier-orbital description of the charge-transfer term is inadequate to explain the directionally of the nucleophilic attack to a carbonyl group. Instead, closed-shell repulsion, electrostatic interactions, and charge transfer must all be taken into account. However, this picture has never been quantitatively verified accurately, and therefore the actual contribution of these critical factors remains unknown. In a different context, we also recently found that the catalysis of various reactions, such as Diels-Alder or Michael addition, is not, as widely accepted, caused by enhancing FMO interactions.[13,14] Instead, our analyses, based on the Activation Strain Model (ASM)[15] and energy decomposition analysis (EDA) method,[16] revealed that catalysis of these reactions is brought about by a reduction in the Pauli repulsion between key occupied molecular orbitals of the reactants. Likewise, Pauli repulsion has been recently found to be behind the directionality of halogen bonds and other electron-rich intermolecular covalent interactions[17] or the bonding in gold(I) complexes.[18] These findings prompted us to quantitatively elucidate the mechanism behind the BD angle and quantify the importance and role of the various physical factors using our ASM-EDA methodology.

Results and Discussion

We first explored the simple addition of cyanide (CN^-) to acetone at the M06-2X/6-311+G(d) level. The reaction proceeds via a reactant complex followed by the transition state and the overall exothermic formation of the adduct (ΔE_R = −3.8 kcal/mol). Geometry optimizations of the transition states associated with the C···C bond formation at different C–C=O angles from 90° to 140° confirm that the optimal angle for the approach of cyanide is indeed obtuse (111.6°, Figure 1). Our calculations not only indicate that the optimal transition state, i.e., the actual first-order saddlepoint **TS-opt**, is more stable than its perpendicular analog, i.e., the constrained **TS-90** ($\Delta\Delta E$ = 12.7 kcal/mol; $\Delta\Delta E$ = 14.8 kcal/mol, at the more accurate DLPNO-CCSD(T)/def2-TZVPP level)[19] but is also reached earlier

[a] H. A. Rodríguez, Prof. Dr. I. Fernández
Departamento de Química Orgánica and Centro de Innovación en Química Avanzada (ORFEO-CINQA)
Facultad de Ciencias Químicas, Universidad Complutense de Madrid
Ciudad Universitaria, 28040-Madrid, Spain
E-mail: israel@quim.ucm.es
[b] H. A. Rodríguez
Instituto de Productos Naturales y Agrobiología (IPNA)
Consejo Superior de Investigaciones Científicas (CSIC)
38206-La Laguna, Tenerife, Spain
[c] Prof. Dr. F. M. Bickelhaupt
Theoretical Chemistry, Department of Chemistry and Pharmaceutical Sciences, Vrije Universiteit Amsterdam, The Netherlands
and
Institute for Molecules and Materials (IMM), Radboud University, Nijmegen, The Netherlands
and
Department of Chemical Sciences, University of Johannesburg, South Africa

Supporting information for this article is available on the WWW under https://doi.org/10.1002/cphc.202300379

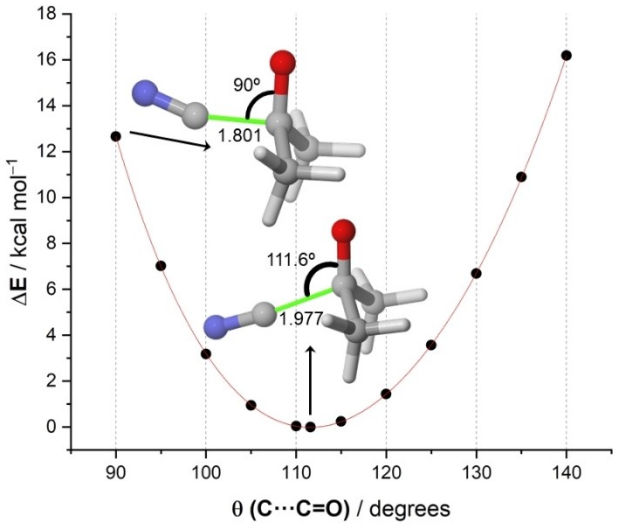

Figure 1. Relative energy (ZPVE included) of the transition states associated with the C···C bond formation at various enforced θ angles. The ball-and-sticks figures represent the fully optimized geometry of the true transition state (**TS-opt**) and the one optimized under the constraint that θ = 90° (**TS-90**). Bond distances are given in angstroms. All data have been computed at the M06-2X/6-311 + G* level.

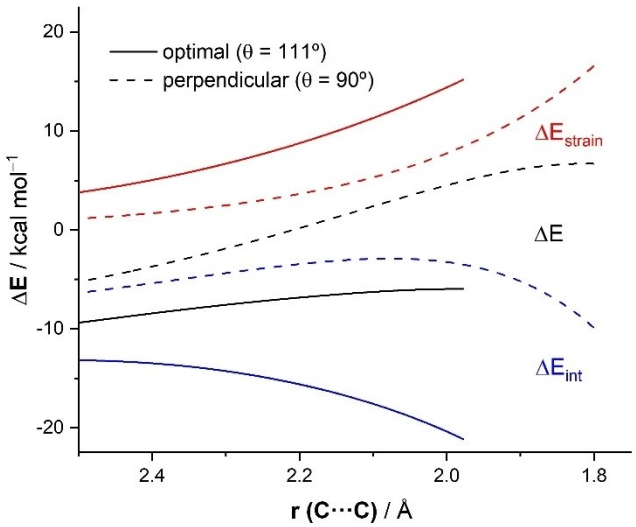

Figure 2. Comparative ASDs of the reaction between $Me_2C{=}O$ and CN^- through the optimal, BD-trajectory (solid lines) and perpendicular approach (dashed lines), projected onto the C···C bond-forming distance and referred to the isolated reactants. All data have been computed at the ZORA-M06-2X/TZ2P//M06-2X/6-311 + G* level.

(C···C(=O) bond-forming distance of 1.977 Å vs 1.801 Å, Figure 1).

Next, the physical factors behind the preference for the obtuse approach over the perpendicular trajectory are analyzed using the Activation Strain Model (ASM).[15] This analysis decomposes the electronic energy (ΔE) into two terms, namely the strain (ΔE_{strain}) that results from the distortion of the individual reactants and the interaction (ΔE_{int}) between the deformed reactants along the reaction coordinate, defined in this case by the NC···C(=O) bond-forming distance.[20] Figure 2 shows the corresponding activation strain diagrams (ASDs) from the initial stages of the transformation up to the respective transition states (**TS-opt** and **TS-90**) for both the obtuse (θ = 111°) and perpendicular (θ = 90°) approaches of the cyanide anion. As readily seen in Figure 2, the perpendicular approach is unfavorable not because of an unfavorable strain ΔE_{strain}, which is actually less destabilizing, but due to a less stabilizing interaction ΔE_{int}. Thus, the more stabilizing interaction ΔE_{int} is the crucial factor rendering the obtuse Bürgi-Dunitz trajectory preferred over the perpendicular approach, from the very beginning of the process and particularly, at the transition state region.

The Energy Decomposition Analysis (EDA)[16] method was applied next to quantitatively understand the factors leading to the stronger interaction energy computed for the preferred BD trajectory. Our canonical EDA involves decomposing the interaction ΔE_{int} between the reactants into three physically meaningful energy terms, namely the classical electrostatic interaction (ΔV_{elstat}), the Pauli repulsion (ΔE_{Pauli}) arising from the repulsion between occupied closed-shell orbitals of both deformed reactants, and the orbital interaction (ΔE_{orb}) that accounts for charge transfer and polarization. From the data in Table 1, it becomes evident that, within this EDA framework, the stronger interaction in the optimal transition state **TS-opt** does not result from stronger electrostatic or orbital attractions, which are actually much stronger in **TS-90**, but exclusively from a less destabilizing Pauli repulsion. One could argue that this significant reduction in ΔE_{Pauli} is a consequence of the longer C···C bond distance in **TS-opt**. For this reason, we also analyzed a related constrainedly-optimized transition state (**TS-90′**) having also perpendicular C–C=O angle but featuring the same consistent C···C bond-forming distance (1.977 Å) as **TS-opt**.[21] As shown in Table 1, **TS-90′** not only exhibits a more destabilizing Pauli repulsion ($\Delta\Delta E_{Pauli}$ = 7.2 kcal/mol), but also slightly less stabilizing electrostatic attractions ($\Delta\Delta V_{elstat}$ = 3.1 kcal/mol), and strikingly, also *less* (not more) stabilizing orbital interactions ($\Delta\Delta E_{orb}$ = 7.4 kcal/mol) than **TS-opt**. Thus, at variance with the traditional view, the BD trajectory also benefits from stronger orbital interactions than the perpendicular trajectory! The same conclusion emerges from the analysis along the entire reaction coordinate, which clearly indicates that the obtuse trajectory benefits from a lower Pauli repulsion and stronger electrostatic and orbital interactions (see Figure 3).

The origin of the reduction in the destabilizing Pauli repulsion for the BD approach was investigated next by

Table 1. EDA terms (in kcal/mol, computed at ZORA-M06-2X/TZ2P//M06-2X/6-311 + G*) of the transition states for the reaction of $Me_2C{=}O$ and CN^-.

System	$\Delta\Delta E^{[a]}$	ΔE_{strain}	ΔE_{int}	ΔV_{elstat}	ΔE_{Pauli}	ΔE_{orb}
TS-opt (111.6°)	0.0 (0.0)	15.2	−21.1	−69.2	113.8	−65.8
TS-90′ (90.0°)	10.8 (11.5)	8.4	−3.5	−66.1	121.0	−58.4
TS-90 (90.0°)	12.7 (14.8)	16.5	−9.8	−105.2	200.0	−104.6

[a] Values within parentheses were computed at the DLPNO-CCSD(T)/def2-TZVPP//M06-2X/6-311 + G* level.

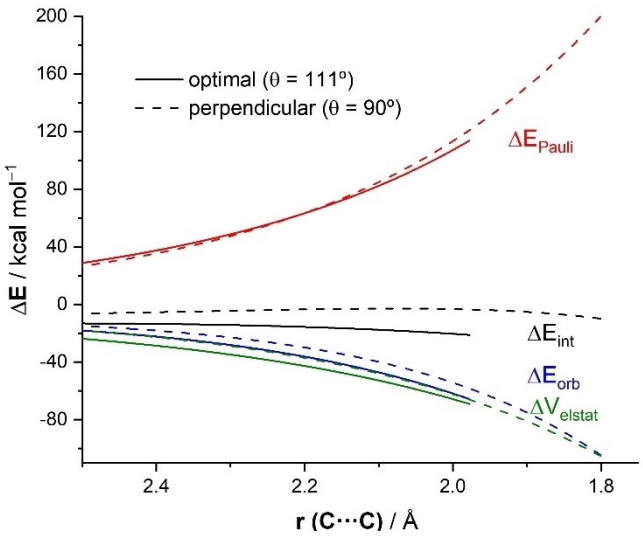

Figure 3. Comparative EDAs of the reaction between $Me_2C{=}O$ and CN^- through the optimal, BD-trajectory (solid lines) and perpendicular approach (dashed lines), projected onto the C···C bond-forming distance and referred to the isolated reactants. All data have been computed at the ZORA-M06-2X/TZ2P//M06-2X/6-311+G* level.

performing a Kohn-Sham molecular orbital (KS-MO) analysis. The main contribution to the Pauli repulsion comes from the four-electron/two-orbital interaction between the occupied HOMO of the nucleophile (i.e. the lone-pair centered at the reactive carbon atom) and the HOMO-1 of the ketone (the π component of the C=O bond, see Figure 4). The orbital overlap between these molecular orbitals is the largest, and therefore, most destabilizing for **TS-90** ($S=0.19$), and smallest and least destabilizing for the optimal **TS-opt** ($S=0.12$), while for **TS-90'** the situation is intermediate ($S=0.14$). The reduction in overlap S, if one goes from perpendicular to obtuse, is the result of moving the lobe of the cyanide HOMO away from the carbonyl π-bonding amplitude of the ketone HOMO-1, and into its nodal surface that occurs when going to the methyl groups. This trend in occupied-occupied overlap translates into the computed ΔE_{Pauli} trend, which decreases from **TS-90** (200 kcal/mol) to **TS-90'** (121.0) and to **TS-opt** (111.3). Therefore, the nucleophile must bend its angle of attack from perpendicular to obtuse in order to minimize an unfavorable Pauli repulsion with the filled π-molecular orbital of the carbonyl group. At wider angles, the Pauli repulsion increases again as a consequence of an increase of the same HOMO/HOMO-1 overlap and also because of repulsion with the occupied σ(C–H) orbitals of the methyl groups of acetone (see Figure S1 in the Supporting Information).

To understand the trend in ΔE_{orb}, we used the Natural Orbital for Chemical Valence (NOCV)[22] extension of the EDA which indicates that the main contribution to ΔE_{orb} (ca. 90%) comes from the HOMO(nucleophile)→π*-LUMO(C=O) (Figure 5). The associated stabilization $\Delta E_{orb}(\varrho 1)$ reveals that this FMO interaction is significantly more stabilizing in **TS-90** than in **TS-opt**, which determines the trend in the overall ΔE_{orb}. Interestingly, the reason is not the widely accepted larger orbital overlap which is actually slightly smaller in **TS-90** ($S=0.33$) than in **TS-opt** ($S=0.35$). This is because, in **TS-90**, the lobe of the nucleophile HOMO begins to cross the nodal surface of the π*-LUMO which goes with cancelation of overlap. Instead, the more stabilizing ΔE_{orb} in **TS-90** originates from the lower orbital energy of the ketone π*-LUMO (−0.64 eV vs −0.55 eV) as a result of the different geometries of these species and also the

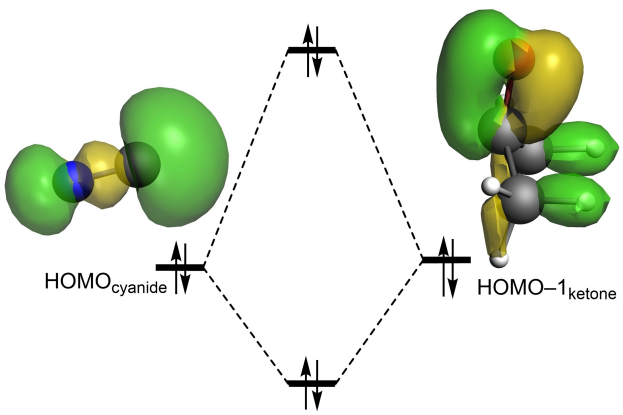

	θ	Orbital Overlap S
TS-90	90°	0.19
TS-90'	90° (opt distance)	0.14
TS	optimal (111°)	0.12

Figure 4. Schematic orbital-interaction diagram of the most significant occupied orbital overlap of the nucleophilic addition reaction of CN^- to $Me_2C{=}O$. All data have been computed at the ZORA-M06-2X/TZ2P//M06-2X/6-311+G* level.

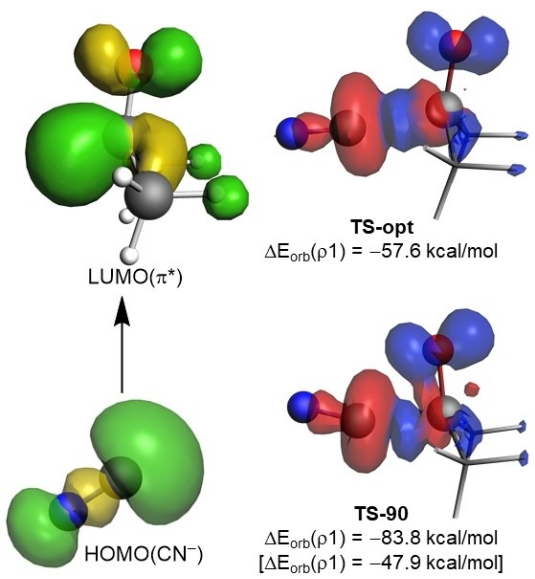

Figure 5. Deformation densities ϱ1 and associated molecular orbitals of the most important orbital interaction $\Delta E_{orb}(\varrho 1)$. Values in brackets refer to **TS-90'**. The color code used to represent the flow of charge is red→blue. All data have been computed at the ZORA-M06-2X/TZ2P//M06-2X/6-311+G* level.

fact that the methyl groups are much less pushed backward and therefore do not amplify the antibonding character between carbonyl and methyl group (Figure 5, top left). Note however that **TS-90′** exhibits the poorest overlap ($S = 0.31$) as well as the highest LUMO (−0.22 eV). The latter ultimately results in the least stabilizing ΔE_{orb}. In other words, a comparison based on consistent C···C distances, i.e. between **TS-opt** and **TS-90′**, yields a picture in which not only ΔE_{Pauli} but also ΔE_{orb} favor the obtuse BD trajectory.

To check the generality of the key role of Pauli repulsion together with more favorable orbital interactions (and electrostatic attractions, albeit to a lesser extent) in defining the optimal BD trajectory of the nucleophilic addition to carbonyl groups, we extended our study to a variety of systems including aldehydes, a differently substituted ketone, the thioketone counterpart of acetone, formic acid and its methyl ester and amide derivatives and also the addition to a conjugated C=C bond in the Michael addition involving pyrrolidine and methyl acrylate (see Table 2). All cases confirm the systematic preference for the obtuse BD angle (ranging from 104.9° to 115.4°) over the perpendicular approach (ΔΔE ranging from 8.8 to 16.6 kcal/mol). Similar results to those obtained for the reaction involving cyanide anion and acetone were found, i.e., in all cases the interaction between the deformed reactants in the optimal transition states is stronger than in their corresponding perpendicular counterparts due to a significant decrease in the ΔE_{Pauli} term. Once again, this is caused by a reduced overlap between the HOMO(nucleophile) and the doubly occupied π-molecular orbital of the carbonyl group. Likewise, the corresponding **TS-90′** transition states (having a perpendicular C–C=O angle but featuring the same consistent bond-forming distance as the optimal **TS-opt**) also exhibit a more destabilizing Pauli repulsion and weaker orbital (and electrostatic, to a lesser extent) interactions. This generalizes the finding that the optimal obtuse BD trajectory emerges mainly from avoiding closed-shell Pauli repulsion but also from more efficient HOMO-LUMO interactions.

As a final support to our findings, we also considered the methyl anion addition from the Grignard species $Me_2Mg(OMe_2)$ to acetone, which has been recently reported to proceed intramolecularly through the initial formation of a complex featuring a C=O···Mg(II) bond.[23] Even in this preorganized complex, the migrating methyl group follows a clear obtuse trajectory (104.9°) where the corresponding transition state lies 10.2 kcal/mol below its perpendicular counterpart. Once again, our EDA calculations, using the deformed $[Me(OMe_2)Mg\cdots O{=}CMe_2]^+$ and CH_3^- as fragments, confirms that the optimal transition state benefits from a reduced Pauli repulsion and more stabilizing orbital interactions (when consistently compared to its **TS-90′** counterpart).

Conclusions

In conclusion, our quantum chemical activation strain analyses at consistent C···C forming distances show that the Bürgi-Dunitz trajectory of a nucleophile adding to a carbonyl group originates from the combined effect of three factors working all in that same direction: i) more favorable electrostatic interactions; ii) a reduced Pauli repulsion between nucleophile HOMO and ketone π(C=O); and iii) more stabilizing HOMO(nucleophile)-π*(C=O) LUMO orbital interactions for the obtuse, *not for the perpendicular*, approach.

Computational Details

Geometry optimizations of the molecules were performed without symmetry constraints using the Gaussian16 (RevB.01) suite of program[24] at the M06-2X[25]/6-311+G* level. Reactants and adducts were characterized by frequency calculations and have positive definite Hessian matrices. Transition states show only one negative eigenvalue in their diagonalized force constant matrices, and their associated eigenvectors were confirmed to correspond to the motion along the reaction coordinate under consideration using the Intrinsic Reaction Coordinate (IRC) method.[26] Energy

Table 2. EDA terms (in kcal mol^{-1}) of the transition states for the reaction of CN^- and different carbonyl groups.[a]

Reaction	System	θ	ΔΔE	ΔE_{int}[b]	ΔE_{Pauli}[b]	ΔV_{elstat}[b]	ΔE_{orb}[b]
$H_2C{=}O + CN^-$	**TS-opt**	115.4°	0.0	−20.9	94.1	−58.2	−56.8
	TS-90	90.0°	15.0	−9.8 (−3.4)	185.6 (100.9)	−97.1 (−55.7)	−98.4 (−48.9)
$Me(H)C{=}O + CN^-$	**TS-opt**	113.3°	0.0	−24.8	104.5	−63.5	−61.6
	TS-90	90.0°	13.7	−4.4 (−7.2)	194.0 (111.2)	−101.2 (−60.6)	−102.3 (−53.9)
$iPr_2C{=}O + CN^-$	**TS-opt**	110.7°	0.0	−25.4	113.9	−71.2	−68.1
	TS-90	90.0°	12.1	−15.0 (−8.6)	205.5 (120.9)	−110.6 (−68.4)	−110.0 (−61.1)
$Me_2C{=}S + CN^-$	**TS-opt**	112.3°	0.0	−15.1	32.9	−23.7	−24.3
	TS-90	90.0°	8.8	−6.8 (−6.6)	78.2 (36.8)	−42.8 (−21.7)	−42.3 (−21.7)
$HCO_2H + CN^-$	**TS-opt**	110.2°	0.0	−20.2	104.4	−64.8	−59.7
	TS-90	90.0°	11.8	−14.4 (−4.5)	222.6 (111.1)	−119.0 (−64.3)	−118.0 (−51.8)
$HCO_2Me + CN^-$	**TS-opt**	109.6°	0.0	−24.1	119.4	−74.2	−69.3
	TS-90	90.0°	12.5	−17.1 (−6.7)	249.3 (129.1)	−132.8 (−73.8)	−133.6 (−62.0)
$HCONH_2 + CN^-$	**TS-opt**	112.0°	0.0	−23.7	185.9	−105.5	−104.1
	TS-90	90.0°	13.2	−10.6 (−4.3)	265.3 (200.5)	−136.4 (−105.8)	−139.6 (−99.0)
pyrrolidine + methyl acrylate	**TS-opt**	110.8	0.0	−9.2	156.8	−85.4	−80.6
	TS-90	90.0°	16.6	1.2 (7.3)	218.5 (192.1)	−111.3 (−97.8)	−106.0 (−87.1)
$Me_2C{=}O + Me_2Mg(OMe_2)$	**TS-opt**	104.9°	0.0	−185.0	108.5	−231.1	−62.4
	TS-90	90.0°	8.0	−171.1 (−177.7)	134.4 (115.8)	−229.1 (−245.3)	−76.4 (−48.2)

[a] Energy values computed at the ZORA-M06-2X/TZ2P//M06-2X/6-311+G* level. [b] Values within parentheses refer to the corresponding **TS-90′** species.

refinements were carried out by means of single-point calculations at the Domain Based Local Pair-Natural Coupled-Cluster (DLPNO-CCSD(T))[27] calculations were performed using Orca 5.0.3[28] using the def2-TZVPP[29] basis set on the M06-2X/6-311+G* geometries. This level is denoted DLPNO-CCSD(T)/def2-TZVPP//M06-2X/6-311+G*.

Activation Strain Model (ASM) of Reactivity and Energy Decomposition Analysis (EDA) Methods

Within the ASM method,[15] the potential energy surface $\Delta E(\zeta)$ is decomposed along the reaction coordinate, ζ, into two contributions, namely the strain $\Delta E_{strain}(\zeta)$ associated with the deformation (or distortion) required by the individual reactants during the process and the interaction $\Delta E_{int}(\zeta)$ between these increasingly deformed reactants:

$$\Delta E(\zeta) = \Delta E_{strain}(\zeta) + \Delta E_{int}(\zeta)$$

The EDA used in this work is based on the method developed by Ziegler and Rauk[30] following a similar procedure suggested by Morokuma,.[31] Within the EDA method,[16] the interaction energy can be further decomposed into the following chemically meaningful terms:

$$\Delta E_{int}(\zeta) = \Delta V_{elstat}(\zeta) + \Delta E_{Pauli}(\zeta) + \Delta E_{orb}(\zeta)$$

The term ΔV_{elstat} corresponds to the classical electrostatic interaction between the unperturbed charge distributions of the deformed reactants and is usually attractive. The Pauli repulsion ΔE_{Pauli} comprises the destabilizing interactions between occupied orbitals and is responsible for any steric repulsion. The orbital interaction ΔE_{orb} accounts for bond pair formation, charge transfer (interaction between occupied orbitals on one moiety with unoccupied orbitals on the other, including HOMO-LUMO interactions), and polarization (empty-occupied orbital mixing on one fragment due to the presence of another fragment). Moreover, the NOCV (Natural Orbital for Chemical Valence)[22] extension of the EDA method has been also used to further partition the ΔE_{orb} term. The EDA-NOCV approach provides pairwise energy contributions for each pair of interacting orbitals to the total bond energy.

The program package ADF[32] was used for EDA calculations using the optimized M06-2X/6-311+G* geometries at the same DFT level in conjunction with a triple-ζ-quality basis set using uncontracted Slater-type orbitals (STOs) augmented by two sets of polarization functions with a frozen-core approximation for the core electrons.[33] Auxiliary sets of s, p, d, f, and g STOs were used to fit the molecular densities and to represent the Coulomb and exchange potentials accurately in each SCF cycle.[34] Scalar relativistic effects were incorporated by applying the zeroth-order regular approximation (ZORA).[35] This level of theory is denoted ZORA-M06-2X/TZ2P//M06-2X/6-311+G*.

Acknowledgements

This work was supported by the Spanish MCIN/AEI/10.13039/501100011033 (Grants PID2019-106184GB-I00 and RED2018-102387-T) and the Dutch Research Council (NWO).

Conflict of Interests

The authors declare no conflict of interest.

Data Availability Statement

The data that support the findings of this study are available in the supplementary material of this article.

Keywords: Bürgi-Dunitz angle · nucleophilic addition · carbonyl · Pauli repulsion · density functional calculations

[1] H.-B. Bürgi, J. D. Dunitz, E. Shefter, *J. Am. Chem. Soc.* **1973**, *95*, 5065–5067.
[2] H.-B. Bürgi, J. M. Lehn, G. Wipff, *J. Am. Chem. Soc.* **1974**, *96*, 1956–1957.
[3] H. B. Bürgi, J. M. Lehn, G. Wipff, *Tetrahedron* **1974**, *30*, 1563–1572.
[4] a) I. Fleming, *Molecular Orbitals and Organic Chemical Reactions*, Chichester: John Wiley & Sons, **2010**; b) A. S. Cieplak, *Organic addition and elimination reactions: Transformation paths of carbonyl derivatives In Structure Correlation*, Vol. 1 (H.-B. Bürgi & J. D. Dunitz, eds.), New York: John Wiley & Sons, **2008**.
[5] a) N. T. Anh, O. Eisenstein, *New J. Chem.* **1977**, *1*, 61–70; b) N. T. Anh, *Top. Curr. Chem.* **1980**, *88*, 145; c) C. H. Heathcock, *Aldrichimica Acta* **1990**, *23*, 94–111.
[6] See, for instance: a) A. Choudhary, D. Gandla, G. R. Krow, R. T. Raines, *J. Am. Chem. Soc.* **2009**, *131*, 7244–7426; b) C. Fufezan, *Proteins* **2010**, *78*, 2831–2838; c) S. H. Light, G. Minasov, M.-E. Dubana, W. F. Anderson, *Acta Crystallogr.* **2014**, *D70*, 544–552; d) N. K. Devaraj, C. L. Perrin, *Chem. Sci.* **2018**, *9*, 1789–1794.
[7] a) G. W. Breton, C. J. Crasto, *J. Org. Chem.* **2015**, *80*, 7375–7384; b) J. Dutta, C. Routray, S. Panday, H. S. Biswal, *Chem. Sci.* **2022**, *13*, 14327–14335; c) J. Echeverría, *Inorg. Chem.* **2018**, *57*, 5429–5437.
[8] A. Bauzá, T. J. Mooibroek, A. Frontera, *Chem. Commun.* **2015**, *51*, 1491–1493.
[9] a) K. Fukui, *Acc. Chem. Res.* **1971**, *4*, 57–64; b) K. Fukui, *Angew. Chem. Int. Ed. Engl.* **1982**, *21*, 801–809.
[10] K. N. Houk, *Theor. Chem. Acc.* **2000**, *103*, 330–331.
[11] See, for instance: a) J. Clayden, N. Greeves, S. Warren, P. Wothers, *Organic Chemistry*. 2nd ed. London, England: Oxford University Press; b) E. V. Anslyn, D. A. Dougherty, *Modern Physical Organic Chemistry*, University Science Books, 2006.
[12] A. J. Stone, R. W. Erskine, *J. Am. Chem. Soc.* **1980**, *102*, 7185–7192.
[13] a) T. A. Hamlin, I. Fernández, F. M. Bickelhaupt, *Angew. Chem. Int. Ed.* **2019**, *58*, 8922–8926; b) P. Vermeeren, T. A. Hamlin, I. Fernández, F. M. Bickelhaupt, *Angew. Chem. Int. Ed.* **2020**, *59*, 6201–6206; c) P. Vermeeren, T. A. Hamlin, I. Fernández, F. M. Bickelhaupt, *Chem. Sci.* **2020**, *11*, 8105–8112.
[14] T. A. Hamlin, F. M. Bickelhaupt, I. Fernández, *Acc. Chem. Res.* **2021**, *54*, 1972–1981.
[15] a) I. Fernández, F. M. Bickelhaupt, *Chem. Soc. Rev.* **2014**, *43*, 4953–4967; b) P. Vermeeren, S. C. C. van der Lubbe, C. Fonseca Guerra, F. M. Bickelhaupt, T. A. Hamlin, *Nat. Protoc.* **2020**, *15*, 649–667; c) F. M. Bickelhaupt, K. N. Houk, *Angew. Chem. Int. Ed.* **2017**, *56*, 10070–10086. See also; d) I. Fernández, in *Discovering the Future of Molecular Sciences* (Ed.: B. Pignataro), Wiley-VCH, Weinheim, **2014**, pp. 165–187.
[16] For reviews on the EDA method, see: a) F. M. Bickelhaupt, E. J. Baerends, in *Reviews in Computational Chemistry*, (Eds. K. B. Lipkowitz, D. B. Boyd), Wiley-VCH: New York, **2000**, Vol. 15, pp. 1–86; b) M. von Hopffgarten, G. Frenking, *WIREs Comput. Mol. Sci.* **2012**, *2*, 43–62; c) I. Fernández, in *Applied Theoretical Organic Chemistry*, (Ed. D. J. Tantillo), World Scientific, New Jersey, **2018**, pp. 191–226.
[17] L. de Azevedo Santos, T. C. Ramalho, T. A. Hamlin, F. M. Bickelhaupt, *Chem. Eur. J.* **2023**, *29*, e202203791.
[18] Z. R. Wong, T. K. Schramm, M. Loipersberger, M. Head-Gordon, F. D. Toste, *Angew. Chem. Int. Ed.* **2022**, *61*, e202202019.
[19] A similar energy difference was computed at the MP2/6-311+G* level ($\Delta\Delta E = 11.9$ kcal/mol), thus further supporting the selected DFT method for this study.

[20] The reaction coordinate was obtained by means of relaxed-scan calculations from the corresponding transition states without modifying the angle of addition. At short C···C distances, this coincides with the corresponding Intrinsic Reaction Coordinate (IRC) calculations.
[21] **TS-90′** was fully TS-optimized with a frozen C···C bond-forming distance of 1.977 Å and $\theta = 90^\circ$ and exhibits only one imaginary vibrational mode.
[22] M. P. Mitoraj, A. Michalak, T. Ziegler, *J. Chem. Theory Comput.* **2009**, *5*, 962–975.
[23] R. M. Peltzer, J. Gauss, O. Eisenstein, M. Cascella, *J. Am. Chem. Soc.* **2020**, *142*, 2984–2994.
[24] Gaussian 16, Revision B.01, M. J. Frisch, G. W. Trucks, H. B. Schlegel, G. E. Scuseria, M. A. Robb, J. R. Cheeseman, G. Scalmani, V. Barone, G. A. Petersson, H. Nakatsuji, X. Li, M. Caricato, A. V. Marenich, J. Bloino, B. G. Janesko, R. Gomperts, B. Mennucci, H. P. Hratchian, J. V. Ortiz, A. F. Izmaylov, J. L. Sonnenberg, D. Williams-Young, F. Ding, F. Lipparini, F. Egidi, J. Goings, B. Peng, A. Petrone, T. Henderson, D. Ranasinghe, V. G. Zakrzewski, J. Gao, N. Rega, G. Zheng, W. Liang, M. Hada, M. Ehara, K. Toyota, R. Fukuda, J. Hasegawa, M. Ishida, T. Nakajima, Y. Honda, O. Kitao, H. Nakai, T. Vreven, K. Throssell, J. A. Montgomery, Jr., J. E. Peralta, F. Ogliaro, M. J. Bearpark, J. J. Heyd, E. N. Brothers, K. N. Kudin, V. N. Staroverov, T. A. Keith, R. Kobayashi, J. Normand, K. Raghavachari, A. P. Rendell, J. C. Burant, S. S. Iyengar, J. Tomasi, M. Cossi, J. M. Millam, M. Klene, C. Adamo, R. Cammi, J. W. Ochterski, R. L. Martin, K. Morokuma, O. Farkas, J. B. Foresman, D. J. Fox, Gaussian, Inc., Wallingford CT, 2016.
[25] Y. Zhao, D. Truhlar, *Theor. Chem. Acc.* **2008**, *120*, 215–241.
[26] C. Gonzalez, H. B. Schlegel, *J. Phys. Chem.* **1990**, *94*, 5523–5527.
[27] C. Riplinger, B. Sandhoefer, A. Hansen, F. Neese, *J. Chem. Phys.* **2013**, *139*, 134101.
[28] F. Neese, *Wiley Interdiscip. Rev.: Comput. Mol. Sci.* **2018**, *8*, e1327.
[29] F. Weigend, R. Ahlrichs, *Phys. Chem. Chem. Phys.* **2005**, *7*, 3297.
[30] T. Ziegler, A. Rauk, *Theor. Chim. Acta* **1977**, *46*, 1–10.
[31] K. Morokuma, *J. Chem. Phys.* **1971**, *55*, 1236–1244.
[32] a) G. te Velde, F. M. Bickelhaupt, E. J. Baerends, C. Fonseca Guerra, S. J. A. van Gisbergen, J. G. Snijders, T. Ziegler, *J. Comput. Chem.* **2001**, *22*, 931–967; b) ADF2020, SCM, Theoretical Chemistry, Vrije Universiteit, Amsterdam, The Netherlands, http://www.scm.com.
[33] J. G. Snijders, P. Vernooijs, E. J. Baerends, *At. Data Nucl. Data Tables* **1981**, *26*, 483–509.
[34] J. Krijn, E. J. Baerends, Fit Functions in the HFS-Method, Internal Report (in Dutch), Vrije Universiteit Amsterdam, The Netherlands, 1984.
[35] a) E. van Lenthe, E. J. Baerends, J. G. Snijders, *J. Chem. Phys.* **1993**, *99*, 4597–4610; b) E. van Lenthe, E. J. Baerends, J. G. Snijders, *J. Chem. Phys.* **1994**, *101*, 9783–9792; c) E. van Lenthe, A. Ehlers, E. J. Baerends, *J. Chem. Phys.* **1999**, *110*, 8943–8953.

Manuscript received: June 1, 2023
Revised manuscript received: June 9, 2023
Accepted manuscript online: June 12, 2023
Version of record online: June 27, 2023